Vol. 23(2) : 195~203 | Ocean and Polar Research | June 2001

# Development of a Nowcast System for the Taiwan Strait (TSNOW): Numerical Simulation of Barotropic Tides

**Sen Jan*[1], Yu-Huai Wang[1], Shenn-Yu Chao[2], and Dong-Ping Wang[3]**

[1]*National Center for Ocean Research*
*P.O. Box 23-13, Taipei 10617, Taiwan, Republic of China*
[2]*Horn Point Laboratory, University of Maryland Center for Environmental Science*
*P.O. Box 0775, Cambridge, MD 21613-0775, USA*
[3]*Marine Science Research Center, State University of New York*
*Stony Brook, NY 11794-5000, USA*

**Abstract** : A fine-grid (3 km×3 km), three-dimensional nowcast system of sea levels, currents, temperature, and salinity is being developed for the Taiwan Strait. The project takes a balanced approach relying equally on models and observations, will have the capacity of real-time data assimilation, and is aimed at both practical and scientific applications. To determine boundary conditions and verify model results, eight coastal tide-gauge stations were first established along both sides of the strait. Strait-wide hydrographic surveys were conducted by research vessels. Currents are being measured using bottom-mounted ADCP moorings in a meridional deep channel off southwest Taiwan and along a traverse section in the central part of the strait. In addition to a fine-resolution three-dimensional model of the Taiwan Strait, an adjoint model and a larger-domain two-dimensional model were used to better determine boundary conditions in the northern and southern boundaries of the strait. In the first stage of model development, barotropic tides were successfully simulated in a hindcast mode. The protocol product has been released to general public, including government agencies, universities and general users.

**Key words** : nowcast system, barotropic tides, numerical model, Taiwan Strait.

## 1. Introduction

In the island of Taiwan, human, industrial and economic activities are intimately linked to the surrounding ocean. The sea brings resources as well as disasters. To minimize negative impacts and manage resources require better understanding of the ocean. In this light, a fine-resolution Taiwan Strait (Fig. 1) nowcast system (TSNOW) has been under development in the National Center for Ocean Research (NCOR) of Taiwan since August 1998. The development of the nowcast system is based on the extensive hydrographic data in the Taiwan Strait and is necessary because of disproportional concentration of Taiwan's population and economy in the west coast. The model development requires timely validation by extensive ship observations that are made possible because of the relatively small size of the Strait. The research task takes a balanced approach relying equally on models and observations, and will have the capacity of real-time data assimilation.

The information about sea levels, ocean currents and frontal locations will be valuable for disaster mitigation, marine rescue missions, environment policy making, fishing industries, and sustainable management of marine resources. To meet these objectives, observations and model development are carried out con-

*Corresponding author. E-mail : jansen@odb03.ncor.ntu.edu.tw

currently. The field observations include sea-level measurements especially at previously unavailable stations along the west side of the Strait, ocean current measurements at mooring stations in the Strait, and strait-wide hydrographic surveys. The model development is divided to three stages. The initial stage is to establish the capability and demonstrate success in doing good hindcast of barotropic tides. Wind-driven part will then be incorporated in the second stage. Mean circulation and baroclinicity will be added in the final stage. Results from observational data and the first stage of model development are described below.

## 2. Observational data

Better understanding of tidal waves is the first step to develop the system. Although tides over the Asian marginal seas have been extensively studied (e.g. Kang *et al.* 1998; Fang *et al.* 1999; Lefevre *et al.* 2000), the dynamics of tides in the Taiwan Strait receives little attention and seems not to be well understood. In this light, tidal sea-level observations and a fine-resolution numerical model is used to examine tides in the Taiwan Strait at first. To determine open-ocean boundary conditions and verify model results, sea levels were measured at 12

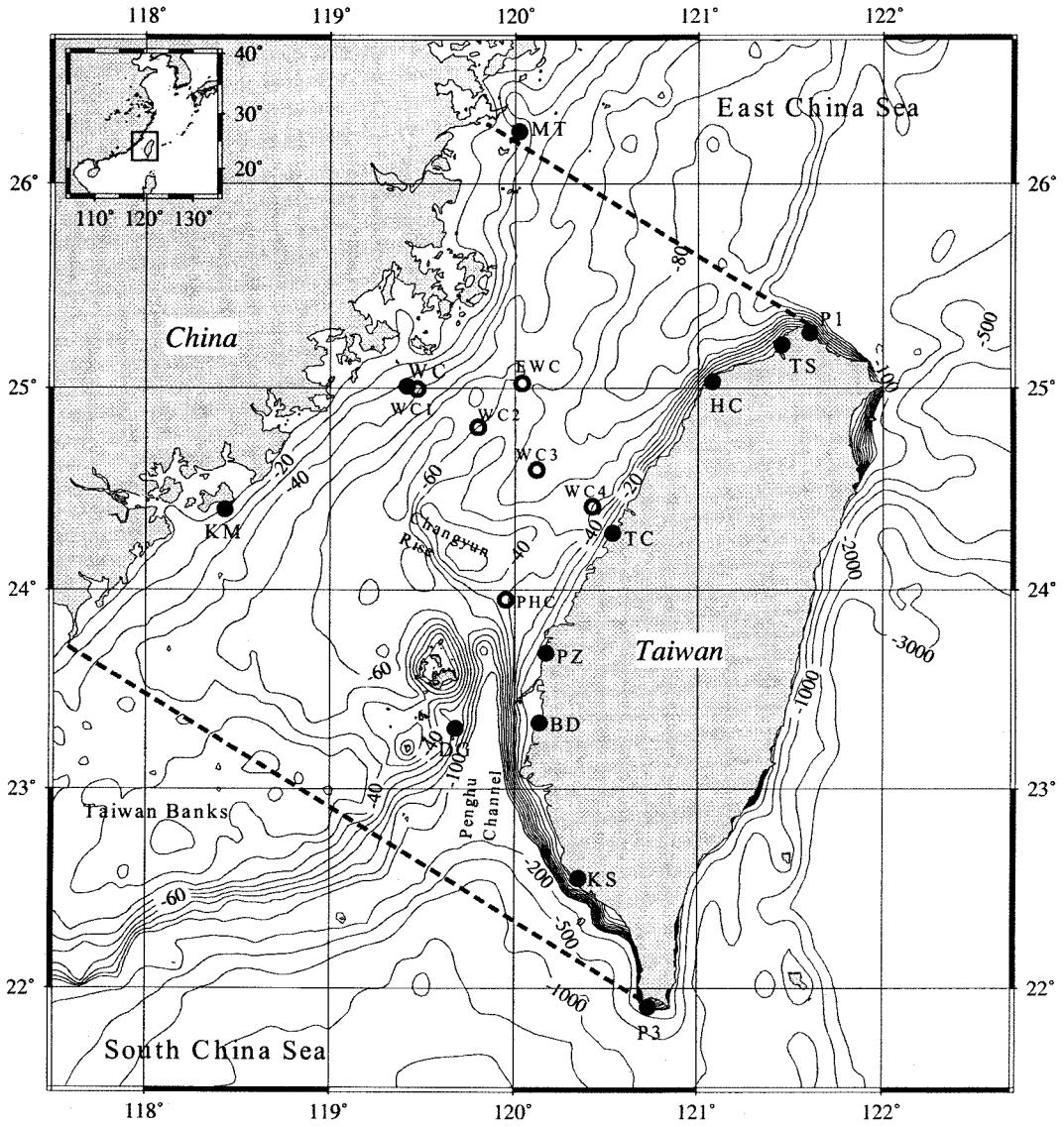


Fig. 1. Bathymetric charts in and around the Taiwan Strait. The full-circle represents tide-gauge stations and open-circle the current meter mooring stations.

Table 1. Harmonic constants for $O_1$, $K_1$, $N_2$, $M_2$, and $S_2$ constituents
(A: amplitude in cm; G: phase in degree; reference time for phase is 0:00 ET 1 January 1901; time basis is GMT).

| Station | Lat. | Long. | $O_1$ | | $K_1$ | | $N_2$ | | $M_2$ | | $S_2$ | |
|---|---|---|---|---|---|---|---|---|---|---|---|---|
| | (° N) | (° E) | A | G | A | G | A | G | A | G | A | G |
| Matsu (MT) | 26° 10′ | 119° 57′ | 25 | 088 | 31 | 120 | 40 | 042 | 210 | 064 | 66 | 096 |
| Wuchou (WC) | 24° 59′ | 119° 27′ | 25 | 112 | 39 | 147 | 35 | 056 | 205 | 089 | 55 | 126 |
| Kinmen (KM) | 24° 24′ | 118° 25′ | 27 | 124 | 33 | 157 | 31 | 091 | 170 | 112 | 49 | 152 |
| Taipowerl (P1) | 25° 18′ | 121° 36′ | 18 | 092 | 21 | 116 | 10 | 045 | 47 | 073 | 12 | 092 |
| Tamsuei (TS) | 25° 11′ | 121° 24′ | 18 | 097 | 20 | 126 | 20 | 061 | 99 | 080 | 30 | 112 |
| Hsinchu (HC) | 24° 51′ | 120° 55′ | 20 | 106 | 23 | 134 | 30 | 064 | 161 | 085 | 47 | 118 |
| Taichung (TC) | 24° 20′ | 120° 33′ | 20 | 115 | 24 | 145 | 33 | 067 | 173 | 090 | 50 | 123 |
| Potzliao (PZ) | 23° 40′ | 120° 08′ | 20 | 125 | 23 | 157 | 18 | 060 | 100 | 081 | 28 | 119 |
| Buda(BD) | 23° 23′ | 120° 09′ | 19 | 126 | 21 | 161 | 12 | 055 | 63 | 075 | 16 | 107 |
| Dongee(DG) | 23° 15′ | 119° 40′ | 19 | 125 | 20 | 159 | 09 | 053 | 50 | 079 | 10 | 112 |
| Kaohsiung (KS) | 22° 37′ | 120° 17′ | 16 | 129 | 18 | 167 | 04 | 333 | 18 | 351 | 07 | 353 |
| Taipower3 (P3) | 21° 57′ | 120° 45′ | 20 | 105 | 21 | 134 | 05 | 309 | 26 | 312 | 11 | 323 |

tide-gauge stations (MT, WC, KM, P1, TS, HC, TC, PZ, DG, BD, KS, and P3 in Fig. 1). The sea-level data, generally recorded longer than one year, were analyzed using Foremans harmonic analysis program (Foreman 1977). Table 1 lists harmonic constants of $O_1$, $K_1$, $N_2$, $M_2$, and $S_2$ for each tide-gauge station. Complex bottom topographic features such as the Taiwan Banks, Changyun Rise, and Penghu Channel off the southwestern Taiwan suggest sizable wave-topography interactions. Characteristic of tidal waves propagation analyzed from harmonic constants listed in Table 1 lends support to this speculation. Overall, tides in the Taiwan Strait are predominantly semidiurnal. The phase of semidiurnal tides increases southward along the China coast from Matsu (MT) to Kinmen (KM), suggesting a southward propagating Kelvin wave. The distance between MT and KM is about 280 km and the phase lag is about 2 hrs between the two stations, leading to a phase speed of about 140 km/hr. In the eastern reaches of the Strait, semidiurnal tides seem to be diffracted from northern and southern tips of Taiwan and converge in the middle reaches off Taichung (TC). Tidal phases vary slowly between Hsinchu (HC) and Potzliao (PZ), indicating a nearly standing wave. Diurnal tides essentially behave as a southward-propagating Kelvin wave passing through the Strait. Amplitudes of semidiurnal tides are relatively large (~ 200 cm) along the west bank between Matsu (MT) and Wuchou (WC), diminishing (< 30 cm) farther southeastward. Summarizing, tidal waves propagate southward in the western reaches and behave as a nearly standing wave in the eastern reaches of the Strait. Conceivably, the coexistence of the two types of waves is related to the complicated bottom features, especially the abrupt deepened topography at the junction of the Taiwan Banks and the northern South China Sea. It is found previous understanding is inadequate for explaining the dynamics of tides in the strait. The dynamics governing the tidal wave propagation is further modulated by long-wave reflection over a topography step (Hilaly 1969; Dean and Dalrymple 1991). Wave reflection occurs when the southward-propagating semidiurnal waves impinge on the steep slope south of the Strait, leading to the coexistence of a progressive wave and a nearly standing wave along the mainland coast and Taiwan coast, respectively. The process has been recently examined (Jan *et al.* 2001).

Thirteen cruises of hydrography survey were conducted on board R/Vs OR1, OR2, and OR3 in 1998-1999. Observed temperature and salinity fields were consistent with those appeared in previous investigations (Jan *et al.* 1994; 1998) except for minor variations. The seasonal variation of flow fields (Fig. 2) in the Strait is briefly described as follow. In winter, the northward intrusion of the Kuroshio Branch Water is severely blocked by the northeast monsoon, and the southward

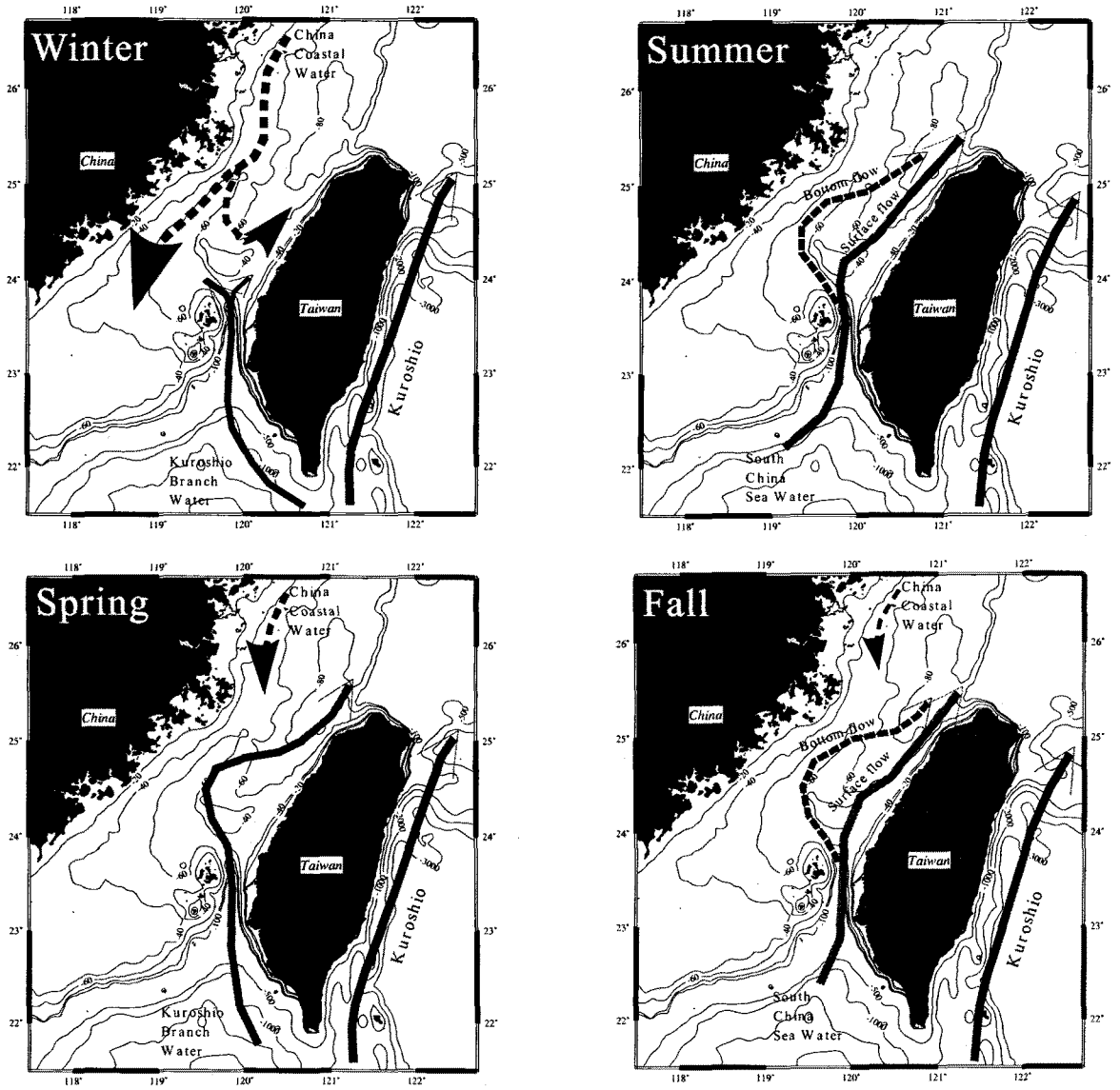


Fig. 2. A schematic showing the seasonal variation of flow fields in the Taiwan Strait.

penetration of the China Coastal Water in the western reaches of the Strait is maximal. A portion of the China Coastal Water is deflected by a zonal rise in the middle of the Strait (the Changyun Rise) and turns back northeastward. In spring, relaxation of northeast monsoon unleashes the northward intrusion of the Kuroshio Branch Water, and the China Coastal Water retreats northward. With the aid of summer stratification and southwest monsoon, the northward intrusion of the South China Sea Water in summer is relatively unimpeded by the Changyun Rise; only the bottom flow is deflected anticyclonically. Further, the China Coastal Water fails to enter the Strait in summer. The fall pattern is similar to the summer pattern, except for the emergence of the China Coastal Water in the northwestern reaches of the Strait. These data will be used in the third stage of model development which will include baroclinic effects.

## 3. Model description

The three-dimensional general circulation model used for this project is similar to that of Semtner (1974) except for the addition of a free surface. The bottom slope is quite large and the baroclinicity is strong in the Strait, justifying the choice of a z-level model over a sigma-

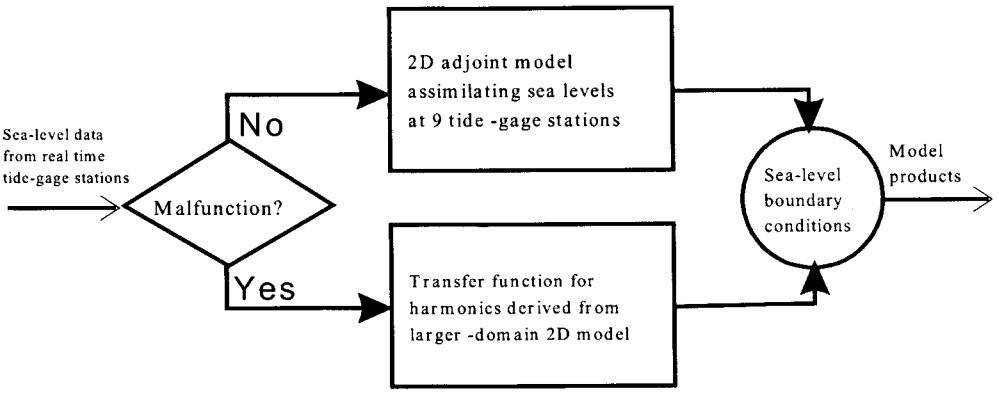


Fig. 3. A schematic showing the relationship between the linear adjoint model and the larger- domain two-dimensional model, and how the two models work for determining sea-level boundary conditions of the nowcast system.

coordinate model (e.g. Princeton Ocean Model) for this nowcast system. The model is formulated under Boussinesq and hydrostatic approximations. It solves for sea levels, temperature, salinity, and velocities in three dimensions. The model domain is bounded by two dashed lines in Fig. 1 with a horizontal grid resolution of 3 km, yielding 127 and 132 grids in the x and y directions, respectively. In the vertical, there are 28 layers and the layer thickness is defined as

$$z(1) = 6.1361 \text{ m}$$
$$z(i) = z(i\text{-}1)/0.9, \; i=2, 28$$

where $z(i)$ is the $i$th layer thickness. The thickness of the top layer fluctuates with sea level variations. The model basin was constructed using a significantly refined (1′ approximately 1.8 km of resolution) depth archive for seas around Taiwan (Liu *et al.* 1998; National Center for Ocean Research of Taiwan 1999). The model basin includes essential topographic features of the Strait.

In the first stage, seawater density was assumed to be homogeneous. Starting from a motionless state, the model was driven by sea-level oscillations on the northern and southern open boundaries. We adopted two approaches to determine sea levels on the two open boundaries. The first one is to use a two-dimensional linear adjont model assimilating sea levels at nine stations (MT, WC, KM, TS, HC, TC, BD, DG, and KS in Fig. 1) to derive the open-boundary sea levels. The second takes advantage of the carefully tuned larger-domain two-dimensional tidal model results (Jan *et al.* 2001). Harmonic constants ($O_1$, $K_1$, $N_2$, $M_2$, and $S_2$) derived from the two-dimensional model on the northern and southern boundaries were linearly correlated to those observed at the northern and southern tips of Taiwan (P1 and P3 in Fig. 1), respectively. Sea levels on the two open boundaries were then extrapolated using harmonic constants analyzed from observed sea levels at P1 and P3. Fig. 4 illustrates the relationship between the adjoint model and the two-dimensional model, and how the two models work for determining sea-level boundary conditions of the nowcast system. Sensitivity tests suggested horizontal and vertical mixing coefficients of $10^7$ cm$^2$/s and 5 cm$^2$/s, respectively, and the non-dimensional bottom drag coefficient of 0.002. Model was driven by sea levels composed of the five major tidal constituents. The harmonic constants derived from the model results were compared with the observations.

## 4. Numerical results

Sea-level variations calculated by the model were processed using harmonic analysis. Fig. 4 shows co-tidal chart and tidal current ellipses of calculated dominant semidiurnal $M_2$ constituent. The co-phase lines in Fig. 4a suggest that the semidiurnal $M_2$ tide behaves as a Kelvin wave propagating southward along the China coast. The phase speed is about 145 km/hr, which is nearly the same magnitude as that derived from observational data in Table 1. In the eastern reach-

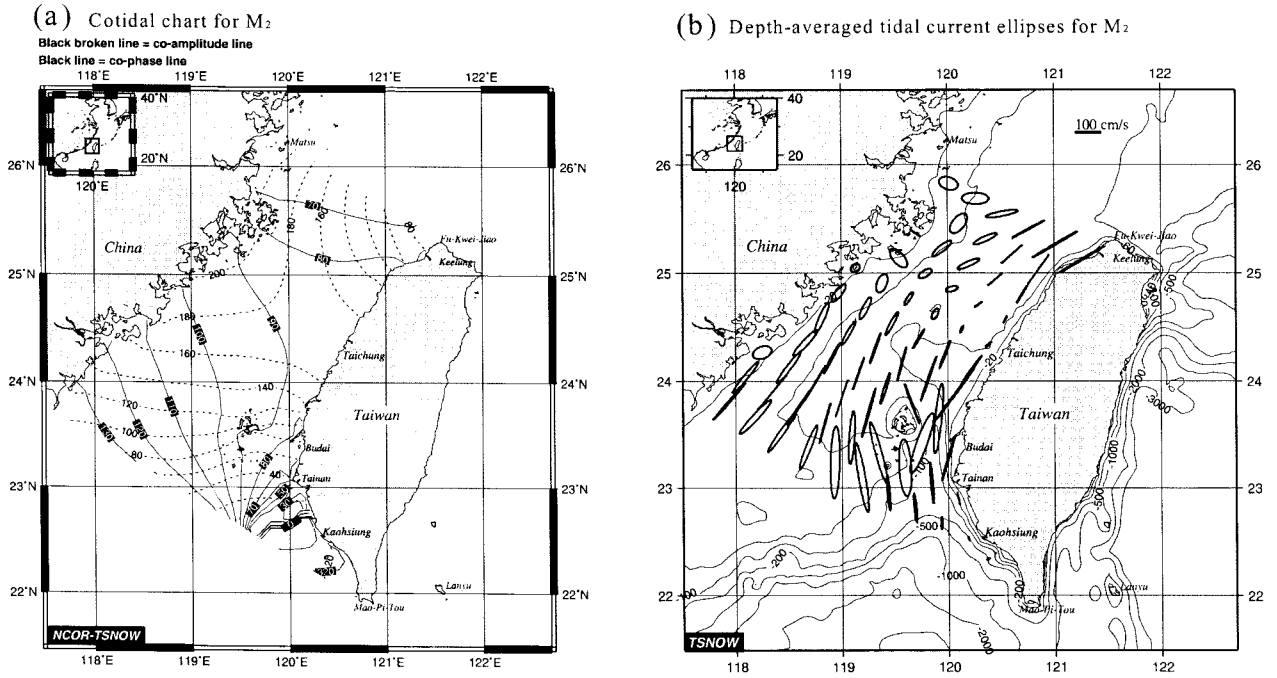


Fig. 4. (a) Co-tidal charts and (b) depth-averaged tidal velocity ellipses for calculated $M_2$ tide in the Taiwan Strait.

es of the Strait, phase angles vary slowly from HC to BD, suggesting a nearly standing wave in this region. The maximum $M_2$ tide amplitude of about 200 cm appears near Wuchou (WC). Tidal current ellipses for $M_2$ tide (Fig. 4b) illustrate strong tidal currents over the Taiwan Banks, off the northwestern Taiwan, and in the Penghu Channel. The maximum tidal current velocity can be as high as 100 cm/s. By comparison, $M_2$ tidal currents are relatively weak in the middle-eastern reaches of the Strait. The relative high amplitudes and weak tidal currents indicate a nearly standing wave in that region.

Fig. 5 shows co-tidal chart and tidal current ellipses of calculated $K_1$ tide. The co-phase lines in Fig. 5a show that the $K_1$ tide propagates southward in the Strait. The amplitudes of $K_1$ tide range from 20 cm to 40 cm in the western reaches, which agrees with that of observational data listed in Table 1. The $K_1$ tidal currents are mostly aligned along the Strait with speeds less than 10 cm/s (Fig. 5b).

To validate simulated tides, sea level data acquired at the nine tide-gauge stations and velocity measured at six bottom-mount ADCP mooring stations (WC1, WC2, WC3, WC4, EWC, and PHC in Fig. 1) were used. The root-mean-squared (RMS) error is widely accepted as a benchmark to evaluate accuracy of simulated tides and is defined as

$$\text{Mean RMS} = \frac{1}{no.\ of\ station} \sum_{station} \sqrt{\left(\frac{1}{T}\sum_{0}^{T}(M-0)^2\right)}$$

where $T$ is the period of tidal constituent, M the time series of model calculated sea-level and O the time series of observed sea-level. Table 2 lists RMS errors averaged over the nine stations for the five major tidal constituents simulated by the adjoint model (ADJM), the three-dimensional model with boundary conditions derived from the two-dimensional model (TSNOW-2D), and the three-dimensional model with boundary conditions derived from the adjoint model (TSNOW-ADJM). Overall, the model performed quite well especially for the dominant $M_2$ constituent (< 12.3 cm). In particular, the RMS errors decrease markedly to a few centimeters if the three-dimensional model is used in conjunction with the adjoint model. The sizable error reduction was made possible because we allow the three-dimensional model to interact with the adjoint model iteratively. Details of the iterative procedures

Table 2. Root-mean-squared errors averaged over the nine stations for five primary constituents simulated by the adjoint Model (ADJM), the TSNOW model with boundary conditions derived from the two-dimensional model (TSNOW-2D), and TSNOW model with boundary conditions derived from the adjoint model (TSNOW-ADJM).

| Models | | Constituents | | | | |
|---|---|---|---|---|---|---|
| | | $M_2$ | $S_2$ | $N_2$ | $K_1$ | $O_1$ |
| ADJM | RMS (cm) | 9.2 | 3.1 | 3.6 | 5.3 | 2.9 |
| TSNOW-2D | RMS (cm) | 12.3 | 11.5 | 2.5 | 9.4 | 2.5 |
| | Model skill | 0.99 | 0.84 | 0.98 | 0.75 | 0.97 |
| TSNOW-ADJM | RMS (cm) | 6.3 | 2.8 | 3.0 | 6.1 | 4.6 |
| | Model skill | 0.99 | 0.99 | 0.98 | 0.89 | 0.91 |

are not presented herein for brevity. For reference, the mean RMS error of the $M_2$ tide is 33 cm for global tidal model results over the East China Sea and is reduced to 15.82 cm for model results of an improved global tidal model over the same area (Lefevre *et al.* 2000). The simulated tidal currents (vertically averaged) ellipses for the five constituents are also in good agreement with the observational data at the six ADCP mooring sites. Observed and calculated $M_2$ and $K_1$ tidal velocity ellipses are shown in Fig. 6, showing reasonable agreements. Table 3 lists depth-averaged tidal current harmonic constants for $K_1$ and $M_2$ constituents, derived from the observations and model results relatively at the six ADCP stations. The overall RMS error, which is a stringent measurement of the model prediction but tends to exaggerate small differences in the orientation and phase, is 5.9 and 9.3 cm/s for $K_1$ and $M_2$, respectively. The percentage of accuracy for $K_1$ is somewhat higher (~ 50 %). However, in practice the absolute error is of the main concern.

We further introduce a model skill factor (MSF) to evaluate model performance, defined as

$$MSF=1-\frac{\varepsilon^2}{\eta^2}$$

in which $\varepsilon^2$ is the error variance between observed and

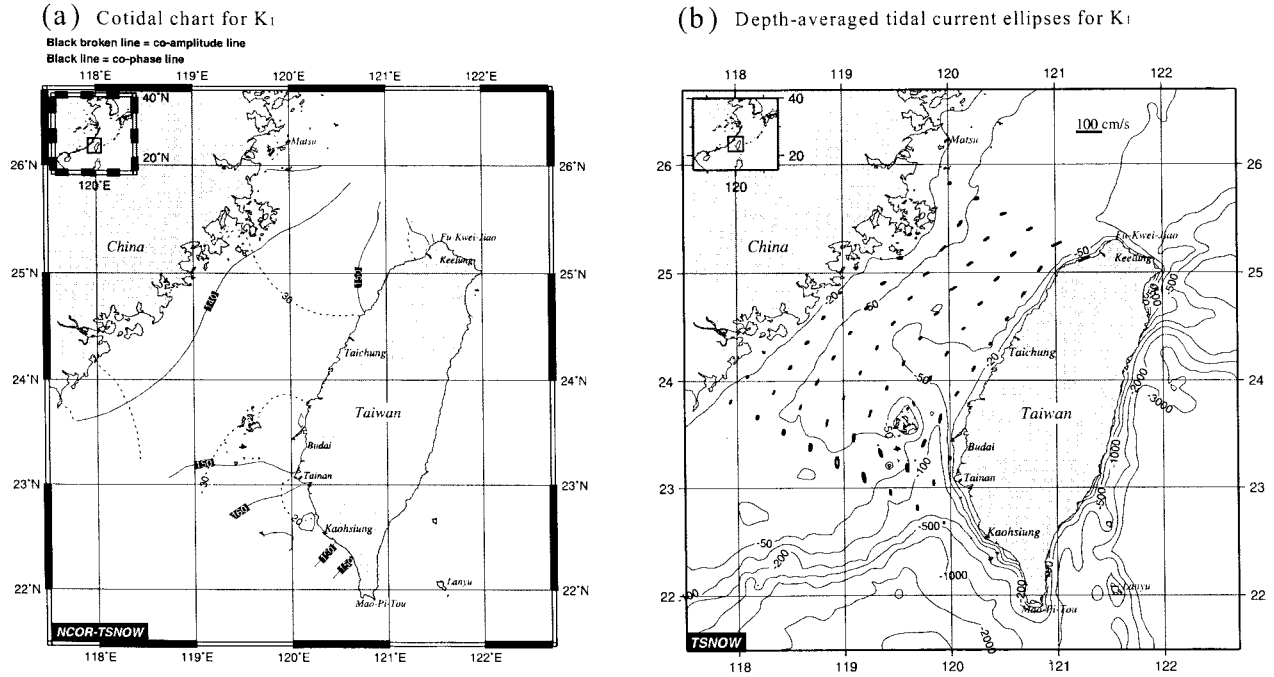


Fig. 5. (a) Co-tidal charts and (b) depth-averaged tidal velocity ellipses for calculated $K_1$ tide in the Taiwan Strait.

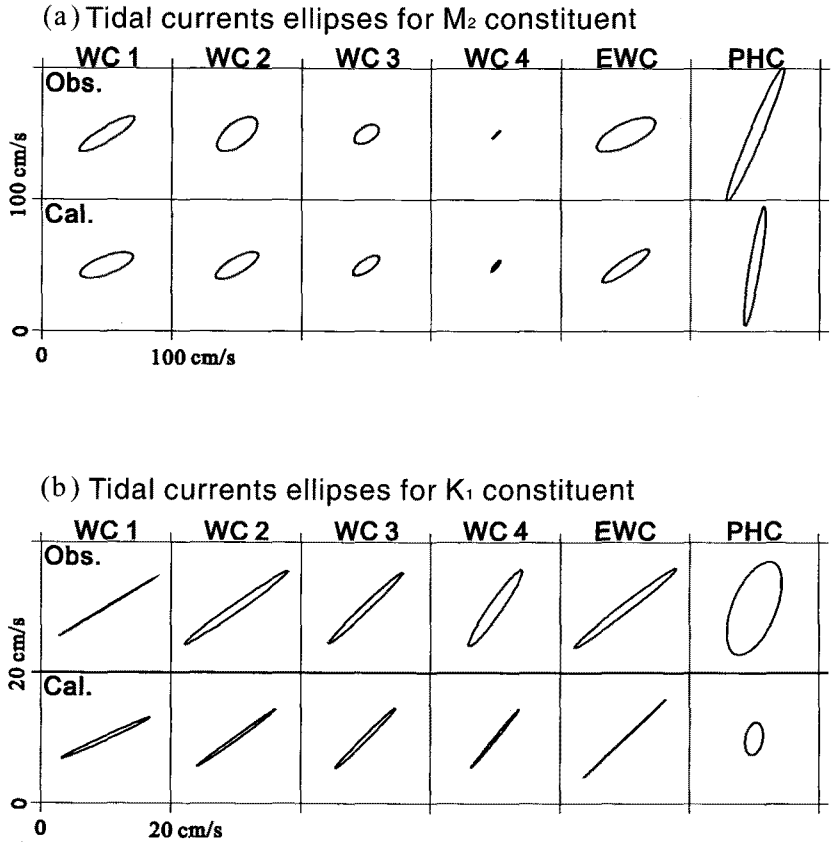


Fig. 6. Comparisons between observed and calculated tidal velocity ellipses for (a) $M_2$ and (b) $K_1$ constituents at six current meter stations (see Fig. 1. for location).

Table 3. Tidal current harmonic constants for $K_1$ and $M_2$ derived from the observations and model results at the 6 ADCP stations (Ma:semi-major axis in cm/s; Mi: semi-minor axis in cm/s; O: orientation in degree; G: phase in degree; time basis is GMT).

| Station | Lat. (° N) | Long. (° E) | Data period (mmyy-mmyy) | Observed | | | | | | | | Simulated | | | | | | | |
|---|---|---|---|---|---|---|---|---|---|---|---|---|---|---|---|---|---|---|---|
| | | | | $K_1$ | | | | $M_2$ | | | | $K_1$ | | | | $M_2$ | | | |
| | | | | Ma | Mi | O | G | Ma | Mi | O | G | Ma | Mi | O | G | Ma | Mi | O | G |
| WC1 | 24° 59′ | 119° 29′ | 0899-1299 | 9.1 | 0.1 | 29 | 305 | 29.5 | 6.5 | 31 | 264 | 4.7 | -1.5 | 5 | 208 | 24.2 | 18.6 | 0 | 239 |
| WC2 | 24° 50′ | 119° 48′ | 0999-1299 | 4.7 | 1.7 | 38 | 238 | 22.1 | 10.5 | 37 | 252 | 6.1 | -0.3 | 20 | 206 | 24.1 | 8.4 | 27 | 251 |
| WC3 | 24° 39′ | 120° 08′ | 0999-1299 | 3.1 | 1.3 | 31 | 223 | 12.7 | 6.8 | 32 | 233 | 6.2 | -0.4 | 30 | 196 | 16.9 | 3.2 | 29 | 235 |
| WC4 | 24° 28′ | 120° 28′ | 0999-1299 | 1.5 | 0.0 | 49 | 213 | 5.3 | 1.0 | 48 | 224 | 7.0 | 0.7 | 56 | 191 | 11.9 | -0.6 | 60 | 211 |
| EWC | 25° 00′ | 120° 08′ | 0799-0999 | 11.3 | 1.0 | 40 | 288 | 31.0 | 11.0 | 25 | 214 | 7.5 | 1.2 | 19 | 204 | 30.6 | 7.0 | 26 | 212 |
| PHC | 23° 51′ | 119° 52′ | 0799-0899 | 7.5 | 3.3 | 69 | 338 | 69.3 | 6.0 | 67 | 348 | 14.5 | -2.4 | 102 | 40 | 57.9 | 4.4 | 81 | 358 |

modeled sea levels, and $\eta^2$ the variance of observed sea levels. The model performance is excellent if MSF is equal to one, and poor if MSF is below 0.5. Table 2 also lists model skill of the two approaches of calculating sea-level boundary conditions for the five major tidal constituents. The model performs quite well, especially for $M_2$ and $N_2$ constituents, for the sea-level boundary conditions either determined by a larger-domain two-dimensional model results or inverted using a linear adjoint model. Model improvements using the two

approaches to determine open boundary conditions is comparable. Both approaches will be useful when the model is used in an operational mode.

## 5. Concluding remarks

In the first stage of model development, barotropic tides were successfully simulated in a hindcast mode. The simulated tides of $O_1$, $K_1$, $N_2$, $M_2$, and $S_2$ constituents agree well with observed sea levels and tidal currents. The model performs equally well when the sea-level open boundary conditions were determined using either an adjoint model or model results derived from a larger domain two-dimensional tidal model. The model also revealed the coexistence of a southward-moving Kelvin wave and a nearly standing wave in the western and eastern reaches of the Strait, respectively. The protocol product has been released to general public, including government agencies, universities, and general users.

In the next stage, the model will include strait-wide, wind-driven circulation, and nearshore tidal residual and buoyancy-driven circulations. The observational strategy, meanwhile, will include long-term ADCP moorings, shallow-water towed-ADCP, and real-time sea level stations. The model results cannot be put to scientific and practical uses before the implementation of wind-driven circulation.

## Acknowledgements

Professors C.-S. Chern, J. Wang, and T.-Y. Tang of Institute of Oceanography, National Taiwan University provided valuable suggestions for this project. Mr. T.-S. Yang, Mr. W.-H. Ho, Mr. B. Wang, Mr. S.-F. Lin, and the crew and technicians of Ocean Research I, II and III assisted the field work. The Central Weather Bureau kindly provided measured sea-level data. Editor of OPR, Dr. K.-I. Chang, reviewer Dr. S.-K. Kang and one anonymous reviewer had contributed substantially to the presentation of the manuscript. This is the National Center for Ocean Research contribution number 33.

## References:

Dean, R.G. and R.A. Dalrymple. 1991. Reflection and transmission past an abrupt transition. p. 141-144. In: *Water Wave Mechanics for Engineers and Scientists.* World Scientific Pub. Co., Singapore, 353 p.

Fang, G., Y.-K. Kwok, K. Yu, and Y. Zhu. 1999. Numerical simulation of principal tidal constituents in the South China Sea, Gulf of Tonkin and Gulf of Thailand. *Cont. Shelf Res.*, 19, 845-869.

Foreman, M. G. G. 1977. *Manual for Tidal Heights Analysis and Prediction.* Pacific Marine Science Report 77-10, Institute for Ocean Sciences, Sidney, Canada.

Hilaly, N. 1969. Water waves over a rectangular channel through a reef. *J. Waterways Harbors Division, ASCE,* 95(WW1), 77-94.

Jan, S., C.-S. Chern, and J. Wang. 1994. A numerical study on currents in Taiwan Strait during summertime. *La Mer,* 32, 225-234.

Jan, S., C.-S. Chern, and J. Wang. 1998. A numerical study of current in the Taiwan Strait during winter. *Terrestrial, Atmospheric and Oceanic Sciences,* 9, 615-632.

Jan, S., C.-S. Chern, J. Wang, S.-Y. Chao, and T.-Y. Tang. 2001. A numerical study on the behavior of tidal waves in the Asian marginal seas. (submitted).

Kang, S.-K., S.-R. Lee, and H.-J. Lie. 1998. Fine grid tidal modeling of the Yellow and East China Seas. *Cont. Shelf Res.*, 18, 739-772.

Lefevre, F., C. Le Provost, and F. H. Lyard. 2000. How can we improve a global ocean tide model at a regional scale? A test on the Yellow Sea and the East China Sea. *J. Geophys. Res.*, 105, 8707-8725.

Liu, C.-S., S.-Y. Liu, S. E. Lallemand, N. Lundberg, and D. L. Reed. 1998. Digital elevation model offshore Taiwan and its tectonic implications. *Terrestrial, Atmospheric and Oceanic Sciences,* 9, 705-738.

National Center for Ocean Research of Taiwan. 1999. TAIDBMv6: Depth Data in Seas around Taiwan. National Science Council, Taipei, Taiwan.

Semtner, A.J. 1986. Finite difference formulation of a world ocean model. p. 187-202. In: *Proceedings of the NATO Advanced Study, Institute on Advanced Physical Oceanographic Numerical Modeling,* ed. by J. J. O'Brien. D. Reidel Pub. Co., Dordrecht.

*Received Mar. 14, 2001*
*Accepted Jun. 30, 2001*